NANO LETTERS

Letter

pubs.acs.org/NanoLett

Gate-Tunable Atomically Thin Lateral MoS_2 Schottky Junction Patterned by Electron Beam

Y. Katagiri,[†] T. Nakamura,[‡] A. Ishii,[§] C. Ohata,[†] M. Hasegawa,[§] S. Katsumoto,[‡] T. Cusati,[∥] A. Fortunelli,[⊥] G. Iannaccone,[∥] G. Fiori,[∥] S. Roche,[#,∇] and J. Haruyama[*,†]

[†]Department of Electrical Engineering and Electronics and [§]Chemistry and Biological Science, Aoyama Gakuin University, 5-10-1 Fuchinobe, Sagamihara, Kanagawa 252-5258, Japan

[‡]Institute for Solid State Physics, The University of Tokyo, 5-1-5 Kashiwanoha, Kashiwa, Chiba 277-8581, Japan

[∥]Dipartimento di Ingegneria dell'Informazione, Università di Pisa, Via G. Caruso, 16, Pisa 56122, Italy

[⊥]CNR-ICCOM, via Giuseppe Moruzzi 1, 56124 Pisa, Italy

[#]Catalan Institute of Nanoscience and Nanotechnology (ICN2), CSIC and The Barcelona Institute of Science and Technology, Campus UAB, Bellaterra, 08193 Barcelona, Spain

[∇]ICREA, Institució Catalana de Recerca i Estudis Avançats, 08070 Barcelona, Spain

Supporting Information

ABSTRACT: Among atomically thin two-dimensional (2D) materials, molybdenum disulfide (MoS_2) is attracting considerable attention because of its direct bandgap in the 2H-semiconducting phase. On the other hand, a 1T-metallic phase has been revealed, bringing complementary application. Recently, thanks to top-down fabrication using electron beam (EB) irradiation techniques, in-plane 1T-metal/2H-semiconductor lateral (Schottky) MoS_2 junctions were demonstrated, opening a path toward the co-integration of active and passive two-dimensional devices. Here, we report the first transport measurements evidencing the formation of a MoS_2 Schottky barrier (SB) junction with barrier height of 0.13–0.18 eV created at the interface between EB-irradiated (1T)/nonirradiated (2H) regions. Our experimental findings, supported by state-of-the-art simulation, reveal unique device fingerprint of SB-based field-effect transistors made from atom-thin 1T layers.

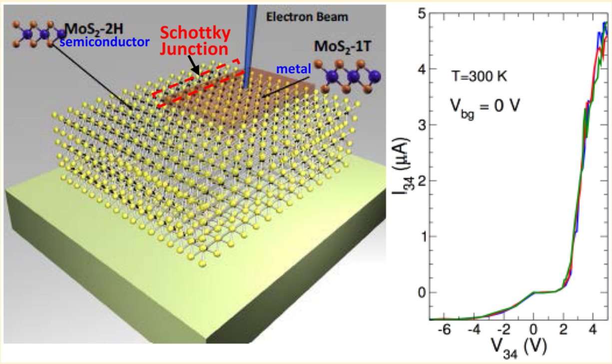

KEYWORDS: *Atomically thin layers, Schottky junction, semiconductor–metal transition, electron-beam irradiation, 1T phase*

MoS_2, one of the transition metal dichalcogenides, is much attractive among atomically thin 2D materials[1−26] because of its direct bandgap of 1.5–1.8 eV in 2H semiconducting phase, especially when atom-thin or flexible circuitry is required. However, the 1T-metallic phase, engineered by chemical doping and laser-beam irradiation, is also useful for some application such as ohmic metallic junction between metal electrode and 2H-MoS_2, and supercapacitor electrode with capacitance value as high as ~700 F/cm^3.[14−19,21] An electronic transition from the 2H (trigonal prismatic D_{3h}) semiconducting to the 1T (octahedral O_h) metal phases of MoS_2 triggered by EB irradiation (see Figure 2e) has been recently observed under the in situ transmission electron microscope (TEM) at high substrate temperature.[12] The two phases can easily be converted from one to the other via intralayer atomic plane gliding, which involves a transversal displacement of one of the S planes (Figure 2e), caused by the charge accumulation and direct momentum transfer from EB combined with substrate heating.

However, to date, such structural observations have not been harnessed to fabricate practical in-plane lateral Schottky junctions and SB devices. It is even unclear whether such lateral SB can be actually formed within atomically thin layers only through atomic-order phase transition. Moreover, if SB devices fabricated with graphene have been already reported, they have been realized with vertically stacked heterostructures via van der Waals engineering and metal/MoS_2 interfacing, which are not suitable for large scale integration.[34−37] The EB-irradiated top-down fabrication of in-plane 1T/2H Schottky junctions[27−30] and SB field effect transistors (SB-FET)[31−33] is highly important because the EB-patterned technique could be in principle scalable to large complex in-plane circuitry. Here, we fabricate this atomically thin EB-patterned lateral MoS_2 Schottky junctions and SB-FET. The device characteristics

Received: March 20, 2016
Revised: May 1, 2016

DOI: 10.1021/acs.nanolett.6b01186
Nano Lett. XXXX, XXX, XXX−XXX

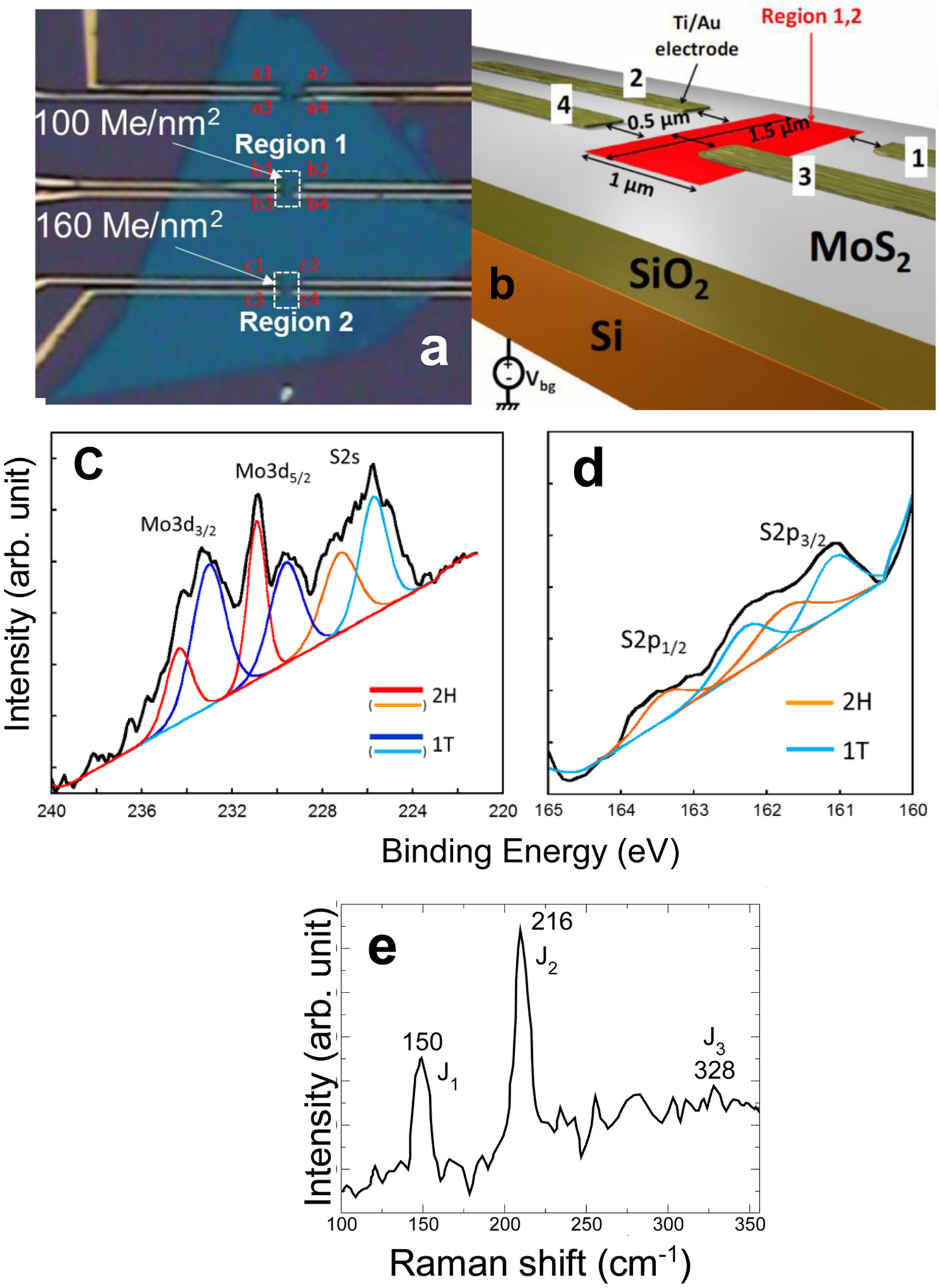

Figure 1. Structural information on few-layer MoS_2 and characterization. (a) Optical microscope image of few-layer MoS_2, mechanically exfoliated from bulk, with two EB irradiation regions and two electrode pairs patterned on individual regions. (b) Schematic view of an electrode pair on one EB-irradiated region of (a). (c,d) XPS spectra of sample shown in (a), which have been measured including the EB-irradiated region 2 and nonirradiated region, showing the Mo 3d S 2s (c) and S 2p (d) peaks of the 1T phases of MoS_2. Typical experimentally measured spectra are shown in black and fits are shown in red (for the 2H phase component) and blue (for the 1T phase component). (e) Typical Raman spectra of EB-irradiated region 2 in (a), showing three peaks unique to the 1T phases of MoS_2.

(with confirmation by X-ray photoelectron spectroscopy (XPS), Raman,[14−20] and photoluminescence (PL) spectroscopies), highlighted by rectification and SB-FET[27−33] properties and supported by first-principles simulations,[38−40] reveal the formation of 2D SBs,[30] which have high tunability by gate-electrostatic-induced doping (0.13−0 eV for back-gate voltage (V_{bg}) of 0−4 V) and are free from Fermi level (E_F) pinning, a fact unique to atomically thin layers with low charge-carrier capability.

In order to create 1T phase embedded into 2H phase, few layer *n*-type MoS_2 flakes with thickness ∼8 nm (∼7 layers) have been fabricated by mechanical exfoliation of bulk MoS_2 following scotch tape method (Figure 1a). Two regions on one sample with individual area of 1.5 × 1 μm^2 have been exposed to EB irradiation with different doses (Figure 1a; 100 Me/nm^2 for region 1 and 160 Me/nm^2 for region 2), without using any dopant at room temperature (see Supporting Information (SI) 1). This was followed by the patterning of two Ti/Au (20 nm/500 nm thick) electrode pairs on individual

DOI: 10.1021/acs.nanolett.6b01186
Nano Lett. XXXX, XXX, XXX−XXX

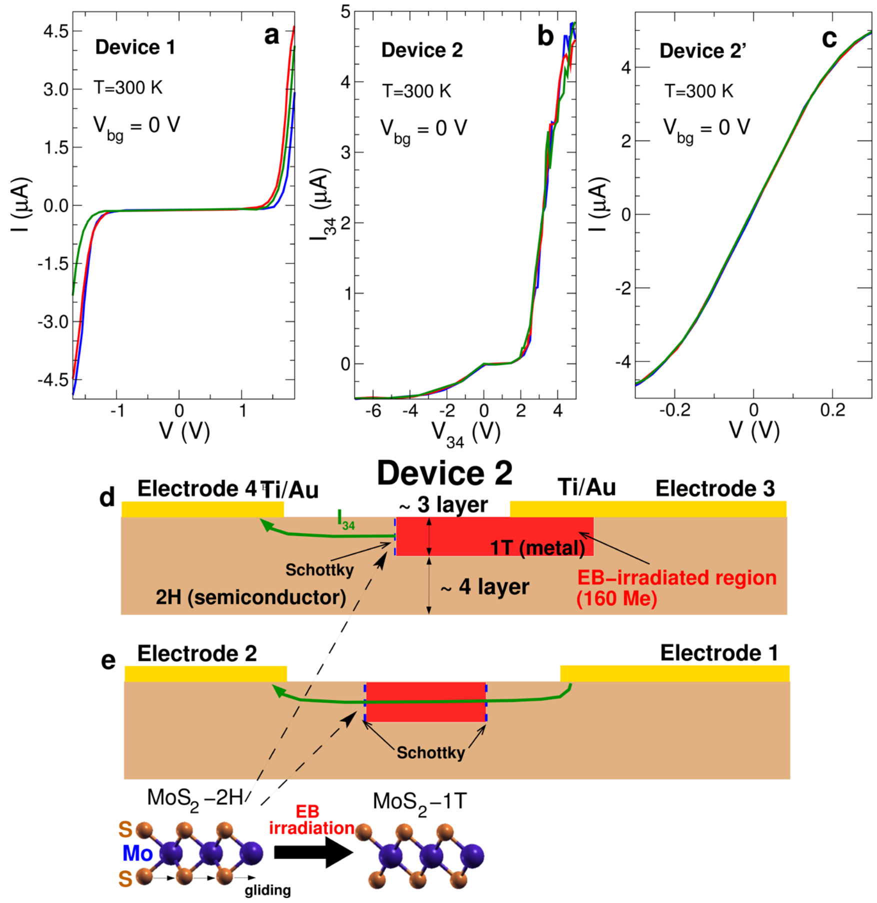

Figure 2. Room-temperature *I* vs *V* relationships for individual electrode pairs formed around two EB-irradiated regions of Figure 1a for (a) Device 1, (b) electrode pair 3−4 of Device 2, and (c) electrode pair formed on EB-irradiated region with 160 Me/nm^2 in another sample (Device 2′). Results of three-times measurements are shown in different colors on individual figures. (d,e) Schematic cross sections of Device 2 for electrode pairs (d) 3−4 and (e) 1−2, corresponding to Figure 1e. Number of layers of ∼4 at bottom-side 2H MoS$_2$ of EB-irradiated region has been confirmed by Raman peak observed around 407 cm^{-1} (A$_{1g}$ peak). That of ∼3 at upper-side 1T MoS$_2$ has been determined by subtracting the 4 layers from total layer number of 7. Inset of (e): Schematic views of two different atomic-structured monolayer MoS$_2$ crystals; 2H semiconducting and 1T metal phases.

regions (Figure 1B). Electrode pair 1−2 is contacted to non-EB-irradiated bulk, while, in the electrode pair 3−4, one electrode is contacted to EB irradiated and the other to non-EB-irradiated bulk. From here on, we will refer to the fabricated device on regions 1 and 2 as Devices 1 and 2, respectively. Back gate electrode was also attached on the back-side of Si substrate with thick SiO$_2$ layer (∼300 nm).

Figure 1c,d show XPS spectra of the sample shown in Figure 1a, measured including the EB- irradiated region 2 and nonirradiated region (see SI 2). The figures show the characteristic Mo 3d S 2s (Figure 1c) and S 2p (Figure 1d) peaks of the 1T phases of MoS$_2$,[14,15] although the larger area of 2H phase results in higher intensity. Typical Raman spectra for EB-irradiated region 2 are also given in Figure 1e. We observe two weak but distinct peaks (i.e., J_1 and J_2 around 150 and 216 cm^{-1}, respectively). These peak positions are in good agreement with previous reports of Raman spectrum for 1T phase MoS$_2$.[16−20] The observed 1T phase is stable even after one month in contradiction to ref 41. One of the possible reasons might be that in our samples, the 1T phase is not free-standing but embedded into 2H phase.

Figure 2 shows the current (*I*) vs voltage (*V*) for two measured devices. Device 1 exhibits symmetric characteristics for both electrode pairs, with non-negligible current in correspondence of $V = \pm 1.5$ V (Figure 2a), as expected for conventional metal−semiconductor−metal structures (i.e., (Ti/Au)/bulk 2H-MoS$_2$/(Ti/Au)).[28] This suggests that the EB-irradiated region in Device 1 does not show any metallic transition and keeps an electronic fingerprint qualitatively similar to bulk MoS$_2$. The EB dose of 100 Me/nm^2 applied to region 1 is too weak to provoke a phase transition. We estimate that the forward voltage (V_F) of our Schottky junction (Ti/Au)/2H-MoS$_2$ is about ∼2 V in Figure 2a (V_F is the voltage at which forward current attains to 4.5 A).

In contrast, I_{34} vs V_{34} characteristics for electrode pair 3−4 of Device 2 strongly differ from those of Device 1 (Figure 2b). Remarkably, a clear asymmetric behavior (i.e., rectification property) is observed with an onset bias voltage of ∼+2.5 V. Such an asymmetric electrical feature can be clearly related to the formation of a Schottky junction,[27] with a barrier height seen by electrons different with respect to that seen by holes. As mentioned above, XPS, Raman, and PL spectra suggest the formation of 1T-phase in EB-irradiated region 2. Because 1T-phase is metallic, the observed Schottky behavior can be explained by the formation of a metal-(1T-phase)/semiconductor (bulk 2H) in-plane junction at the surface within ∼3 layers (Figure 2d). Indeed, an electrode pair in contact with ed to a region irradiated by an EB with dose of 160 Me/nm^2 in another sample (Device 2′) actually exhibits a metallic characteristic (i.e., a symmetric behavior showing no rectification property) (Figure 2C). Moreover, electrode pair 1−2 of Device 2 does not drive any current (i.e., $I_{12} < \pm 200$ nA at $V_{12} < \pm 5$ V). This supports the presence of two Schottky junctions with large barrier heights between electrodes 1 and 2 in Device 2 (Figure 2e) because reverse bias voltage regime for applied V_{12} (i.e., corresponding to $-V_{34}$ regime of Device 2 in Figure 2b) is dominant for the symmetrically placed two Schottky junctions. In Figure 2b, V_F is as large as ∼5 V. This is much larger than $V_F = 2$ V of the (Ti/Au)/2H-MoS$_2$ junction shown in Figure 2a. Since V_F is basically proportional to Schottky barrier height, the Schottky barrier height for Figure 2b is thus different as compared to that of the (Ti/Au)/2H-MoS$_2$ junction, and hence, the Schottky barrier for Figure 2b is attributed to 2*H*/1T phase junction. From the V_F value in Figure 2a, the barrier height of (Ti/Au)/2H-phase is estimated to be as small as 0.05−0.07 eV, when that for 2H/1T is estimated to be 0.13−0.18 eV from Figure 4 in latter part.

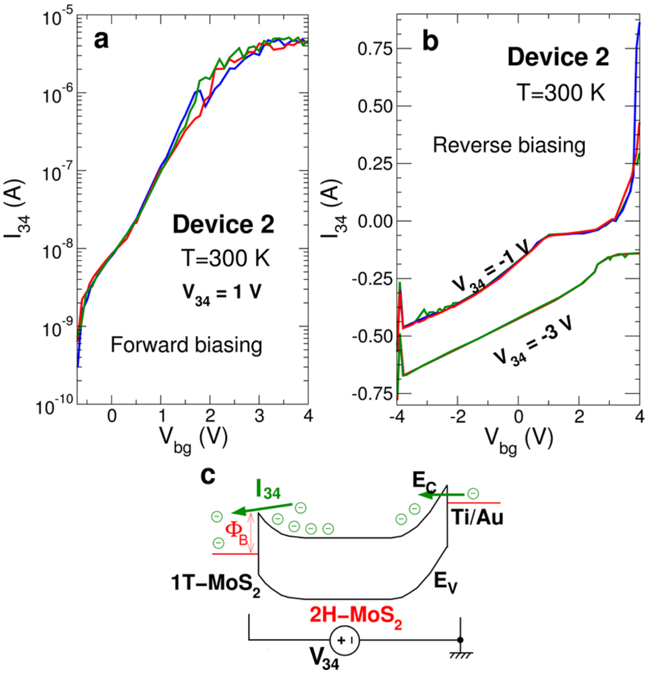

Figure 3. Room-temperature back-gate voltage (V_{bg}) dependence of Figure 2b (electrode pair 3−4 in Device 2). (a,b) I_{34} vs V_{bg} relationships for the forward (a) and reverse (b) V_{34}. *Y*-axis of (a) is a logarithmic. Results of three-time measurements are shown in different colors on individual figures. Note that current limiter of the measurement facility is set to 5 μA through all measurements. (c) Schematic energy band diagrams of Schottky barrier (SB) FET consisting of (1T-metal)/(2H-semiconductor)/(Ti/Au electrode 3) under forward bias voltage ($+V_{34}$) and $+V_{bg}$.

Next, we focus on the electrical characteristics of electrode pair 3−4 in Device 2, as a function of V_{34} for different V_{bg} (Figure 2d). Figure 3a shows typical logarithmic I_{34} vs V_{bg} characteristics for $V_{34} = +1$ V (i.e., forward bias voltage region). Under $+V_{bg}$, these characteristics resemble that of a n-type SB-FET,[31−33] which consists of (1T-MoS$_2$ metal)/2H-MoS$_2$ n-semiconductor/(Ti/Au electrode) (Figure 3c). As $+V_{bg}$ increases, the barrier at the Schottky contacts is thinned, and electrons can easily flow from the right contact to the channel and eventually to the left contact, increasing I_{34}. As it can be seen in Figure 3a, the current is modulated over 4 orders of magnitude ($I_{on}/I_{off} \approx 10^4$) and the subthreshold slope (*SS*) is approximately 1 V/decade. The obtained *SS* is almost the same as that observed in CNT-SB-FET and SB-MOSFET with SB height of 0.3 eV and thick back gate oxide.[32,33] This also supports the formation of a SB in Device 2.

Figure 3b shows I_{34} vs V_{bg} characteristics for two different reverse biases (i.e., $V_{34} = -1$ and -3 V). As can be seen, larger currents are observed for $V_{34} = -3$ V. This might stem from various possible mechanisms, such as the reduction of the barrier height driven by electron accumulation in the 1T-MoS$_2$ metal reservoir, image-force lowering, or contribution of tunneling current, all this certainly deserves future investigation for integrating practical devices with fully control characteristics on large circuit area.

Figure 4a−c shows Arrhenius plots for I_{34} normalized over temperature (i.e., $I_{34}/T^{3/2}$ for 2D Schottky junction formula given by eqs 1−4) for different V_{bg} (V_{bg} = 0, 4, and 2 V, respectively) and fixed $V_{34} = -2$ V (i.e., reverse bias). For Figure 4a, I_{34} linearly decreases below $1/T_c = 0.0067$ as $1/T$ value increases (i.e., I_{34} increases at critical T (T_c) > 150 K with increasing T), while I_{34} significantly drops to above $1/T_c$. In contrast, in Figure 4b, for $1/T$ smaller than $1/T_c$ (i.e., high T), the curve becomes constant (i.e., T-independent). This can be explained by the facts that for large V_{bg} the SB becomes almost transparent and that thermal energy does not significantly contribute to increase I_{34} (as explained for Figures 4d,e, and 5e).

The experimental data (Figure 4a,b) are analyzed using the expression of the current (I) in a 2D Schottky diode as a function of T.[30]

$$I = I_{2D}[\exp(qV/\eta k_B T) - 1] \tag{1}$$

$$I_{2D} = W A^*_{2D} T^{3/2} \exp\left(-\frac{q\phi_B}{k_B T}\right) \tag{2}$$

$$A^*_{2D} = q\sqrt{8\pi k_B{}^2 m^*/h^2} \tag{3}$$

$$m^* = 0.45 m_0 \tag{4}$$

where η is the diode ideality factor (i.e., takes into account the presence of generation/recombination phenomena), A^*_{2D} is the 2D Richardson constant, W (= 1.5 μm) is the junction length, Φ_B is the SB height, k_B is the Boltzmann constant, m^* is the effective mass of MoS$_2$, and m_0 is the mass of electron. When a negative V_{SD} (corresponding to $-V_{34}$ in our device) is applied, eq 1 results in $I = -I_{2D}$. Thus, the T-dependence of I_{SD} agrees with the T-dependence given by eq 2.

The linear relationships obtained in Figure 4a,b support the validity of eq 2 describing the formation of a Schottky junction at the interface between EB-irradiated/nonirradiated (bulk) regions of Device 2, although other physical origins have not been considered as mentioned above. The best fits using eqs 2−4 (dotted lines) give $\Phi_{B1} \approx 0.13$ eV at $1/T < 0.0067$ K^{-1} and $\Phi_{B2} \approx 0.18$ eV at $1/T > 0.0067$ K^{-1} in Figure 4a, and $\Phi_{B3} \approx 0.15$ eV at $1/T > 0.0067$ K^{-1} in Figure 4b, when total area of the Schottky junction $S = 2500$ nm^2 and $\eta = 1.07$ are used. The result $\eta = 1.07$ suggests the presence of a small amount of generation/recombination current at the junction, possibly owing to defects introduced by the EB irradiation.

For Figure 4a, one of the origins of two SB with heights Φ_B estimated at temperatures above and below T_c can be

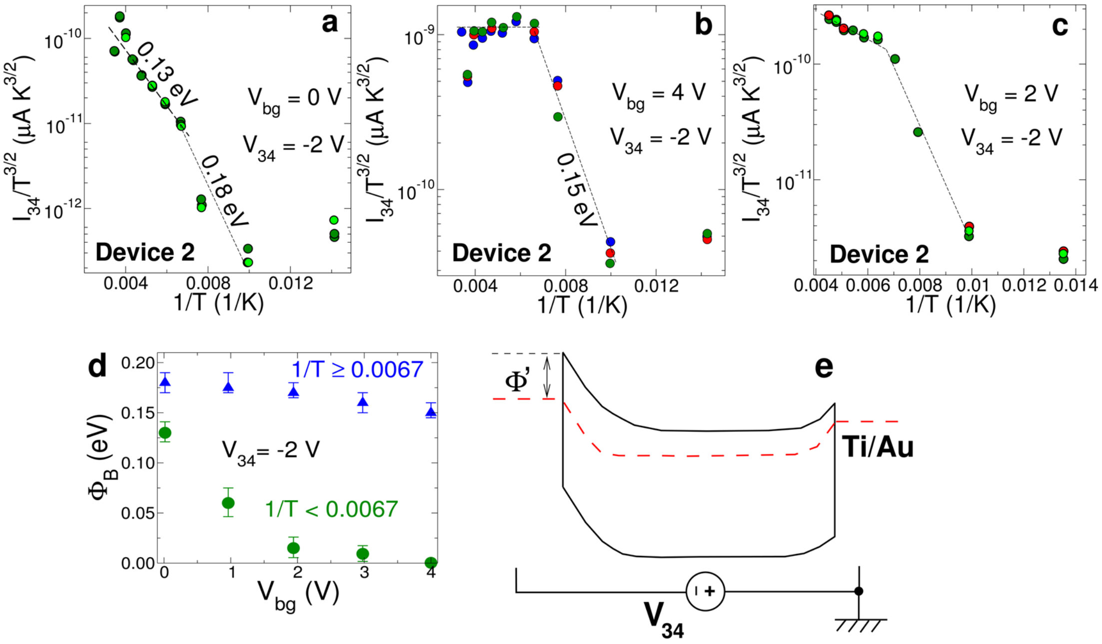

Figure 4. Temperature dependence of I_{34} (Arrhenius plot and 2D Schottky formula) of Figure 3a and gate tunability. (a,b) I_{34} normalized by temperature ($I_{34}/T^{3/2}$) vs $1/T$ at $V_{bg} = 0$ V (a) and 4 V (b) under fixed $V_{34} = -2$ V. (c) That for intermediate $V_{bg} = 2$ V under $V_{34} = -2$ V. Dotted lines are obtained by data fitting using eqs 1–4. (d) Gate-tunability of Φ_B for high (circle plots) and low (triangle plots) temperatures, including results of (a)–(c). The error bars show the results of three samples (SI 3). (e) Schematic energy band of 1T/2H-phase MoS$_2$ Schottky junction under reverse bias voltage ($-V_{34}$) and $+V_{bg}$ to explain (d).

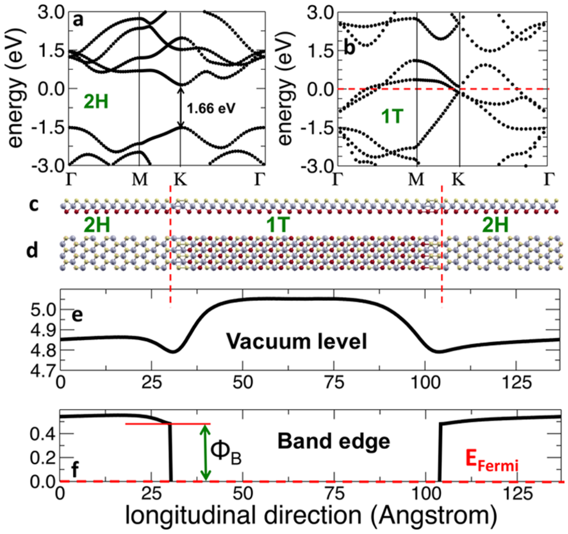

Figure 5. Calculation results based on density functional theory (DFT). (a) 2H-MoS$_2$ monolayer bands. (b) 1T-MoS$_2$ monolayer bands. (c) Side and (d) top atomistic schematic representation of the 2H/1T/2H MoS$_2$ heterostructure. (e) Vacuum level and (f) band edges of the structure, as computed from DFT calculations. E_F of the heterostructure has been considered as the reference potential for both potentials shown in (e) and (f).

understood from the obtained two S values, which give the best fits. $\Phi_{B1} \approx 0.13$ eV at $1/T < 0.0067$ and $\Phi_{B2} \approx 0.18$ eV at $1/T > 0.0067$ give S = 5 nm × 300 and 5 nm × 200 nm, respectively. For Figure 4b, an interesting T-independent $\Phi_B \approx 0$ eV at $1/T < 0.0067$ K^{-1} is observed. Figure 4c exhibits a result at intermediate V_{bg} (= +2 V) between Figure 4a ($V_{bg} = 0$) and b (V_{bg} = +4 V). $\Phi_B \approx 0.015$ eV at $1/T < 0.0067$ K^{-1} actually corresponds to intermediate value. Including these results, Figure 4d (shown by circle plots) reveals the high sensitivity of Φ_B to applied V_{bg} at high temperatures, implying highly gate-tunable Φ_B (SI 3). In contrast, data reported in Figure 4d as triangle plots suggest the low sensitivity of Φ_B to applied V_{bg} at low temperatures (SI 3). The possible origins of this different behavior will be discussed later, in connection with Figures 4e and 5e.

To deepen the analysis of the 2H/1T interface, we have performed DFT calculations, considering the geometry of 2H/1T MoS$_2$ interfaces as experimentally observed with atomistic details given in ref 12. This approach allows us to obtain accurate information on the SB forming at the 2H/1T interface, taking into account both the band offset and the formation of dipoles. We neglect the possible contribution of interface defects or recombination centers, which are likely present (suggested experimentally by the Schottky factor η = 1.07, which is larger than 1 and can provide localized states affecting the SB. First-principles DFT calculations are performed using the Quantum Espresso package,[38] utilizing a plane wave basis set, a gradient-corrected exchange-correlation functional,[39] and scalar-relativistic ultrasoft pseudopotentials (US-PPs)[40] (SI 4). Figure 5a,b show the computed bands for monolayer 1T and 2H-phase MoS$_2$, respectively. Exploiting the information in ref 12, we built a periodic model of a 2H/1T/2H heterojunction whose atomistic structure is shown in Figure 5c,d, which represents a realistic model of a 1T-phase embedded within the generating 2H phase.

Figure 5e shows a plot of the vacuum level potential profile with respect to E_F showing the formation of dipoles at the heterointerfaces. DFT calculations provide a value of 0.73 eV for the energy difference between the electron affinity of 2H MoS$_2$ and the work function of 1T MoS$_2$. From this information, we plot in Figure 5f the conduction band edge profile in the structure relative to the E_F and extract a Φ_B of 0.47 eV, in reasonably good agreement with the experimental results. The residual discrepancy between predicted and observed values of the Schottky barrier can be ascribed to several effects. One likely effect is the change in the work function of the 1T phase due to doping by the contact electrode: indeed, from test calculations we found that such a doping induces an upward shift in the background potential of the 1T phase by ∼0.3−0.4 eV, which could easily account for the observed discrepancy (see SI 5). Other possibilities include the mentioned defects and recombination centers at the interface, which can induce midgap states, thus reducing the effective Φ_B. Indeed, a dependence of the Shottky barrier on the work function has been observed in other Schottky junctions: for example, the Φ_B of non-hydrogenated and hydrogenated Pd/few-layer MoS_2 SBs were reported to be 0.25 and 0.15 eV, respectively. Hydrogenation of Pd reduced the work function of Pd and subsequently reduced the Φ_B to ∼0.1 eV.[31] Moreover, a value of 0.3 eV for Φ_B was reported in SB-MOSFET with *S* value (∼1 V/decade) similar to ours as mentioned above.[32]

One can also see in Figure 5e that the potential in the 1T phase shows some variations at the interface because 1T MoS_2 has a relatively low density of states (in this sense it is not an ideal metal). This also may explain the observed highly V_{bg}-sensitive Φ_B at high temperatures (circle plots in Figure 4d). In this hypothesis, in fact, as the V_{bg} is increased, electrons doped from substrate accumulate in the 1T-phase region under $-V_{34}$, increasing E_F with respect to the conduction band, hence decreasing Φ_B to Φ_B', which is an effective barrier height assuming contribution of only thermionic current and ignoring effects like tunneling and band bending. When E_F in the 1T-metal region coincides with the top of the Schottky junction by further increasing V_{bg}, Φ_B' becomes zero, and thus, electrons feel no SB. Therefore, a T-independent zero-Φ_B value appears. The dependence of Φ_B on T is likely to depend on the energy and nature of localized states at the heterointerface. If confirmed by future studies, this tunable Fermi level E_F, highly sensitive to electrostatic carrier doping via back-gate electrode, would be unique to the present SB consisting of 1T phase of atomically thin (∼3 layers) MoS_2. It would also implies that the E_F is almost free from pinning by defects at the SB despite of the presence of generation/recombination center, particularly in the high T regime. This would be also a significant benefit of the atomically thin layers in which pinned E_F can be easily shifted by increased electrostatic potentials induced by the accumulation of the doped charge carriers in 1T area. This high tunability can be highly useful in future atomically thin in-plane device applications. Reduction of the barrier height due to image-force lowering caused by V_{bg} may also contribute to Figure 4d. Moreover, tunneling current caused by the thinning of the SB at the large V_{bg} may be another origin for the T-independent behavior observed in Figure 4b.

However, in the low temperature region Φ_B is almost insensitive to V_{bg} (triangle plots in Figure 4d). This might be understood by the presence of defects nearby the other SB-junction, which could have been accidentally introduced during fabrication process, resulting in an E_F pinning.

In conclusion, we demonstrated the first EB-patterned gate-tunable in-plane atomically thin Schottky junction and SB-FET fabricated with a top-down approach, by inducing a structural phase change in few-layer MoS_2 through an EB irradiation dose of 160 Me/nm^2 at room temperature. Observation of XPS, Raman, and PL spectra exhibit presence of 1T metallic phase on the EB irradiated region. Experimental measurements and ab initio simulations provide a coherent physical picture of the properties of the 2D Schottky junction created at the interface of EB-irradiated (1T)/nonirradiated (2H) regions. The difference between the experimentally observed SB height (∼0.13−0.18 eV) and the one obtained by theory (0.47 eV) can be explained by the shift in the work function of the 1T phase due to doping by the contact electrode, although the presence of defects and recombination centers introduced by EB irradiation might also play a role. Our findings, supported by state-of-the-art simulations, also indicate a possibility that the effective barrier height is highly sensitive to electrostatic charge doping and almost free from E_F pinning when assuming predominance of the thermionic current contribution. However, more efforts are needed to fully confirm the variability of the SB characteristics with temperature and V_{bg} (e.g., the presence of the two different SB junctions and contribution of defects) and to establish the atomic-scale in-plane SB devices as building blocks of 2D electronic and optoelectronic circuits. This EB top-down patterning opens the possibility to fabricate in-plane lateral heterostructure FETs,[9] which have shown promising scaling prospects in the nanometer range,[10] and/or local interconnects directly with metallic phase (1T) between $(2H)MoS_2$ transistors, resulting in ultimate flexible and wearable in-plane integration circuits without using 3D metal wirings.[42−44]

■ ASSOCIATED CONTENT

Ⓢ Supporting Information

The Supporting Information is available free of charge on the ACS Publications website at DOI: 10.1021/acs.nanolett.6b01186.

> Conditions for EB irradiation, XPS observation, temperature dependence of electrical characteristics, and simulation methods (PDF)

■ AUTHOR INFORMATION

Corresponding Author

*E-mail J-haru@ee.aoyama.ac.jp.

Author Contributions

Y. K., T. N., A. I., C. O., and Y.K.F. performed experiments. T.C., A. F., G.I., and G.F. performed theoretical calculation. J.H., S.K., T.N., M.H. designed the experiments. J.H. and A.I. analyzed the data. J.H., T.C., A.F., S.R., G.I., and G.F. wrote the manuscript.

Notes

The authors declare no competing financial interest.

■ ACKNOWLEDGMENTS

The authors thank T. Inoue, S. Chiashi, S. Maruyama, Y. Shimazaki, T. Yamamoto, S. Tarucha, S. Murakami, Y. Otani, T. Enoki, and T. Ando for their technical contribution, fruitful discussions, and encouragement. This work at Aoyama Gakuin was partly supported by a Grant-in-aid for Scientific Research (Basic Research A: 24241046 and Challenging Exploratory Research: 15K13277) and grant for private University in MEXT and AOARD grant (135049) in U.S. Air Force Office of Scientific Research. The Tokyo University's work was also supported by the Special Coordination Funds for Promoting Science and Technology. Computational resources at nanohub.org are gratefully acknowledged. S. Roche acknowledges support from the Severo Ochoa Program (MINECO, Grant No. SEV-2013-0295). G.Iannacconne, Gianluca Fiori and Stephan Roche acknowledge the funding from the European

Union Seventh Framework Programme under Grant agreement No. 604391 Graphene Flagship.

REFERENCES

(1) Novoselov, K. S.; Geim, A. K.; Morozov, S. V.; Jiang, D.; Zhang, Y.; Dubonos, S. V.; Grigorieva, I. V.; Firsov, A. A. *Science* **2004**, *306*, 666.

(2) Geim, A. K.; Grigorieva, I. V. V *Nature* **2013**, *499*, 419−425.

(3) Roy, T.; Tosun, M.; Kang, J. S.; Sachid, A. B.; Desai, S. B.; Hettick, M.; Hu, C. C.; Javey, A. *ACS Nano* **2014**, *8*, 6259.

(4) Li, L.; Yu, Y.; Ye, G. J.; Ge, O.; Ou, X.; Wu, H.; Feng, D.; Chen, X. H.; Zhang, Y. *Nat. Nanotechnol.* **2014**, *9*, 372.

(5) Churchill, H. O. H.; Herrero, P.-J. *Nat. Nanotechnol.* **2014**, *9*, 330.

(6) Ferrari, A. C.; Bonaccorso, F.; Falko, V.; Novoselov, K. S.; Roche, S.; et al. *Nanoscale* **2015**, *7*, 4598−4810.

(7) Kang, K.; Xie, S.; Huang, Li.; Han, Y.; Huang, P. Y.; Fai Mak, K.; Kim.; et al. *Nature* **2015**, *520*, 656.

(8) Fiori, G.; Iannaccone, G.; Palacios, T.; Neumaier, D.; Seabaugh, A.; Banerjee, S. K.; Colombo, L. *Nat. Nanotechnol.* **2014**, *9*, 768−779.

(9) Fiori, G.; Betti, A.; Bruzzone, S.; Iannaccone, G. *ACS Nano* **2012**, *6*, 2642−2648.

(10) Logoteta, D.; Fiori, G.; Iannaccone, G. *Sci. Rep.* **2014**, *4* (6607), 1−6.

(11) Levendorf, M. P.; Kim, C.-J.; Brown, L.; Huang, P. Y.; Havener, R. W.; Muller, D. A.; Park, J. *Nature* **2012**, *488*, 627−632.

(12) Lin, Y.-C.; Dumcenco, D. O.; Huang, Y.-S.; Suenaga, K. *Nat. Nanotechnol.* **2014**, *9*, 391−396.

(13) Eda, G.; Fujita, T.; Yamaguchi, H.; Voiry, D.; Chen, M.; Chhowalla, M. *ACS Nano* **2012**, *6*, 7311−7317.

(14) Acerce, M.; Voiry, D.; Chhowalla, M. *Nat. Nanotechnol.* **2015**, *10*, 313−318.

(15) Kappera, R.; Voiry, D.; Yalcin, S. E.; Branch, B.; Gupta, G.; Mohite, A. D.; Chhowalla, M. *Nat. Mater.* **2014**, *13*, 1128−1134.

(16) Jiang, L. F.; Zhang, S. L.; Kulinich, S. A.; Song, X. F.; Zhu, J. W.; Wang, X.; Zeng, H. B. *Mater. Res. Lett.* **2015**, *3* (4), 177−183.

(17) Guo, Y.; Sun, D.; Ouyang, B.; Raja, A.; Song, J.; Heinz, T. F.; Brus, L. E. *Nano Lett.* **2015**, *15* (8), 5081−5088.

(18) Nayak, A. P.; Akinwande, D.; et al. *Nano Lett.* **2015**, *15* (1), 346−353.

(19) Liu, Q.; Li, X.; He, Q.; Khalil, A.; Liu, D.; Xiang, T.; Wu, X.; Song, L.; et al. *Small* **2015**, *11* (41), 5556−5564.

(20) Splendiani, A.; Sun, L.; Zhang, Y.; Li, T.; Kim, J.; Chim, C. Y.; Galli, G.; Wang, F. *Nano Lett.* **2010**, *10*, 1271−1275.

(21) Cho, S.; et al. *Science* **2015**, *349*, 625−628.

(22) Lee, C.-H.; et al. *Nat. Nanotechnol.* **2014**, *9*, 676−681.

(23) Hong, X.; Kim, J.; et al. *Nat. Nanotechnol.* **2014**, *9*, 682.

(24) Choi, M. S.; Lee, G. H.; Yu, Y. J.; Lee, D. Y.; Lee, S. H.; Kim, P.; Hone, J.; Yoo, W. J. *Nat. Commun.* **2013**, *4*, 1624.

(25) Wang, H.; Yu, L.; Lee, Y. H.; Shi, Y.; Hsu, A.; Chin, M. L.; Li, L. J.; Dubey, M.; Kong, J.; Palacios, T. *Nano Lett.* **2012**, *12*, 4674.

(26) Radisavljevic, B.; Radenovic, A.; Brivio, J.; Giacometti, V.; Kis, A. *Nat. Nanotechnol.* **2011**, *6*, 147−150.

(27) Sze, S. M.; Ng, K. K. *Physics of Semiconductor Devices*, 3rd ed; Wiley: 2006.

(28) Fontana, M.; Deppe, T.; Boyd, A. K.; Rinzan, M.; Liu, A. Y.; Paranjape, M.; Barbara, P. *Sci. Rep.* **2013**, *3*, 1634.

(29) Lince, J. R.; Carre, D. J.; Fleischauer, P. D. *Phys. Rev. B: Condens. Matter Mater. Phys.* **1987**, *36*, 1647−1656.

(30) Anwar, A.; Nabet, B.; Culp, J.; Castro, F. *J. Appl. Phys.* **1999**, *85*, 2663.

(31) Javey, A.; Guo, J.; Wang, Q.; Lundstrom, M.; Dai, H. *Nature* **2003**, *424*, 654.

(32) Appenzeller, J.; Knoch, J.; Derycke, V.; Martel, R.; Wind, S.; Avouris, Ph. *Phys. Rev. Lett.* **2002**, *89*, 126801.

(33) Heinze, S.; Tersoff, J.; Martel, R.; Derycke, V.; Appenzeller, J.; Avouris, Ph. *Phys. Rev. Lett.* **2002**, *89*, 106801.

(34) Yang, H.; et al. *Science* **2012**, *336*, 1140−1143.

(35) Britnell, L.; et al. *Science* **2012**, *335*, 947−950.

(36) Chen, C.-C.; Aykol, M.; Chang, C. − C.; Levi, A. F. J.; Cronin, S. B. *Nano Lett.* **2011**, *11*, 1863−1867.

(37) Yu, Y.-J.; Zhao, Y.; Ryu, S.; Brus, L. E.; Kim, K. S.; Kim, P. *Nano Lett.* **2009**, *9*, 3430−3434.

(38) Giannozzi, P.; et al. *J. Phys.: Condens. Matter* **2009**, *21*, 395502.

(39) Perdew, J.; Burke, K.; Ernzerhof, M. *Phys. Rev. Lett.* **1996**, *77*, 3865.

(40) Vanderbilt, D. *Phys. Rev. B: Condens. Matter Mater. Phys.* **1990**, *41*, 7892.

(41) Qian, X.; Liu, J.; Fu, L.; Li, J. *Science* **2014**, *346*, 1344.

(42) Haruyama, J. Special Issue on "Carbon Nanoelectronics". *Electronics* **2013**, *2* (4), 368−386.

(43) Hashimoto, T.; Kamikawa, S.; Haruyama, J.; Soriano, D.; Pedersen, J. G.; Roche, S. *Appl. Phys. Lett.* **2014**, *105*, 183111.

(44) Shimizu, T.; Haruyama, J.; Marcano, D. C.; Kosynkin, D. V.; Tour, J. M.; Hirose, K.; Suenaga, K. *Nat. Nanotechnol.* **2011**, *6*, 45−50.

DOI: 10.1021/acs.nanolett.6b01186
Nano Lett. XXXX, XXX, XXX−XXX